Quantum Dynamics of Hydride Transfer in Enzyme Catalysis

Cristobal Alhambra, José C. Corchado, Maria Luz Sánchez, Jiali Gao,* and Donald G. Truhlar*

Contribution from the Department of Chemistry and Supercomputer Institute, University of Minnesota, Minneapolis, Minnesota 55455-0341

Received April 27, 2000

Abstract: One of the strongest experimental indications of hydrogen tunneling in biology has been the elevated Swain−Schaad exponent for the secondary kinetic isotope effect in the hydride-transfer step catalyzed by liver alcohol dehydrogenase. This process has been simulated using canonical variational transition-state theory for overbarrier dynamics and optimized multidimensional paths for tunneling. Semiclassical quantum effects on the dynamics are included on a 21-atom substrate−enzyme−coenzyme primary zone embedded in the potential of a substrate−enzyme−coenzyme−solvent secondary zone. The potential energy surface is calculated by treating 54 atoms by quantum mechanical electronic structure methods and 5506 protein, coenzyme, and solvent atoms by molecular mechanical force fields. We find an elevated Swain−Schaad exponent for the secondary kinetic isotope effect and generally good agreement with other experimental observables. Quantum mechanical tunneling is calculated to account for ∼60% of the reactive flux, confirming the dominance of tunneling that was inferred from the Swain−Schaad exponent. The calculations provide a detailed picture of the origin of the kinetic isotope effect and the nature of the tunneling process.

Introduction

Over the last several years, experimental studies of kinetic isotope effects have led to increased appreciation of the role of quantum mechanical tunneling effects in enzyme kinetics.[1−4] The strongest experimental evidence for hydrogen tunneling in biology has been based primarily on the Swain−Schaad exponent for secondary kinetic isotope effects in the hydride-transfer step in liver alcohol dehydrogenase (LADH) catalysis (the Swain−Schaad exponent, defined below, relates the D/T rate constant to the H/T rate constant). Although the importance of quantum mechanical tunneling and zero point energy effects in small-molecule kinetics is widely appreciated,[5] and models of quantum effects in enzyme kinetics have been advanced for a long time,[6] most simulations[7] of protein dynamics have been restricted to classical molecular dynamics.[8,9] It is of great interest to gain insights into the role of quantum mechanical tunneling in biological systems. Two questions are directly relevant: (1) Can kinetic isotope effects be accurately predicted for enzymatic processes? (2) To what extent does quantum mechanical tunneling contribute to the rate enhancement in LADH? In this report, we use a combined quantum mechanical and molecular mechanical (QM/MM) potential energy function in semiclassical quantum dynamics simulations and demonstrate how this method can be used for the computation of kinetic isotope effects and Swain−Schaad exponents in enzymatic reactions. We find an elevated Swain−Schaad exponent for the secondary kinetic isotope effect in LADH catalysis. The quantitative results provide a detailed picture of the nature of the tunneling process.

For large systems, the most promising methods for including quantum mechanical nuclear-motion effects in dynamical processes are based on semiclassical theory in which the quantum effects are approximated by the leading corrections to the classical limit, as in the well-known Wilson−Sommefeld−Einstein rule for quantization of bound motions and the Wentzel−Kramers−Brillouin (WKB) approximation for unbound wave functions. The classical-limit quantum mechanical result for a tunneling probability is $\exp(-2\theta/\hbar)$, where θ is the imaginary action integral along an analytically continued trajectory that penetrates the barrier to rearrangement.[10] The least action variational principle for tunneling finds the highest-probability tunneling path for each total energy as the path that minimizes the exponential decay by the best compromise of low effective mass, low barrier, and short path for the motion

* Corresponding authors. E-mail: gao@chem.umn.edu or truhlar@umn.edu.

(1) Cha, Y.; Murray, C. J.; Klinman, J. P. *Science* **1989**, *243*, 1325.

(2) Bahnson, B. J.; Park, D.-H.; Kim, K.; Plapp, B. V.; Klinman, J. P. *Biochemistry* **1993**, *32*, 5503. Bahnson, B. J.; Klinman, J. P. *Methods Enzymol.* **1995**, *249*, 373.

(3) Bahnson, B. J.; Colby, T. D.; Chin, J. K.; Goldstein, B. M.; Klinman, J. P. *Proc. Natl. Acad. Sci. U.S.A.* **1997**, *94*, 12797. Kohen, A.; Klinman, J. P. *Acc. Chem. Res.* **1998**, *31*, 397. Kohen, A.; Klinman, J. P. *Chem. Biol.* **1999**, *6*, R191.

(4) Cho, Y.-K.; Northrop, D. B. *Biochemistry* **1999**, *38*, 7470.

(5) Johnston, H. S. *Gas-Phase Reaction Rate Theory*; Ronald Press: New York, 1966.

(6) See, e.g., Marcus, R. A. In *Tunneling in Biological Systems*; Chance, B., et al., Eds.; Academic: New York, 1979; p 109. Sumi, H.; Ulstrup, J. *Biochim. Biophys. Acta* **1988**, *26*, 955. Hynes, J. T. In *The Enzyme Catalysis Process*; Cooper, A., Houben, J. L., Chien, L. C., Eds.; Plenum: New York, 1989; p 293. Bruno, W. J.; Bialek, W. *Biophys. J.* **1992**, *63*, 689.

(7) Significant exceptions are the inclusion of quantum mechanical corrections on 5 or 18 modes of the substrate or water by Feynman path integrals (Hwang, J.-K.; Chu, Z. T.; Yadav, A.; Warshel, A. *J. Am. Chem. Soc.* **1991**, *95*, 8445. Hwang, J.-K.; Warshel, A. *J. Am. Chem. Soc.* **1996**, *118*, 11745), on 3 modes of the substrate by multiconfigurational surface hopping (Decornez, H.; Drukker, K.; Hurley, M. M.; Hammes-Schiffer, S. *Ber. Bunsen-Ges. Phys. Chem.* **1998**, *102*, 533), and on 75 modes of the substrate and protein by small-curvature multidimensional tunneling calculations in ref 22. The latter calculations treated most of the modes of the protein dynamically in only one of the two stages of the calculation, while treatments with less quantum mechanical degrees of freedom treated more modes by classical dynamics in all stages of the calculation.

(8) Brooks, C. L. III; Karplus, M.; Pettitt, B. M. *Adv. Chem. Phys.* **1988**, *71*, 1.

(9) Stanton, R. V.; Miller, D. L.; Kollman, P. A. In *Modern Methods for Multidimensional Dynamics Computations in Chemistry*; World Scientific: Singapore, 1998; p 355.

10.1021/ja001476l CCC: $19.00
Published on Web 08/12/2000

that takes the system through the classically forbidden region of coordinates.[11] A key feature of such motions is that they involve corner cutting as compared to the motion along a curved minimum-energy path through the multidimensional coordinate space.[12−14] A practical approximation called optimized multidimensional tunneling (OMT) approximates the optimum tunneling path by variationally comparing tunneling probabilities computed from action integrals appropriate in the limits of small reaction-path curvature (with mild corner cutting) and large reaction-path curvature (in which a straight-line motion leads to the shortest path with the maximum corner cutting).[15] The OMT approximation has been validated by extensive comparison to accurate quantal dynamics for small systems,[16] but—unlike converged quantum dynamics calculations—it remains doable for large systems.

To calculate an actual reaction rate also requires a method for estimating overbarrier contributions, and both the overbarrier and tunneling calculations require a Born−Oppenheimer potential energy surface (PES) whose gradient is the force field. In the present study, overbarrier processes are calculated by quantized canonical variational theory (CVT),[17] and the final rate constant calculated here (denoted CVT/OMT) is equal to the CVT one (which corresponds to classical reaction-coordinate motion) times the OMT transmission coefficient κ (which accounts for the competition between tunneling and overbarrier processes by incorporating the quantal character of reaction-coordinate motion). Note that the full quantum mechanical description includes both overbarrier and tunneling processes, but CVT with $\kappa = 1$ includes only the former. The PES is calculated by a combined QM/MM approach.[18−21] It has recently been demonstrated that this combination provides a practical way to include quantum effects in molecular dynamics simulations of enzyme rate constants.[22]

LADH is a dimeric enzyme that requires nicotinamide adenine dinucleotide (NAD^+) as a coenzyme. Each unit of the dimer has 374 residues and 2 Zn atoms (one structural and one catalytic). The present simulation includes the benzyl alcoholate substrate, the coenzyme, 260 residues, 2 Zn atoms, and 534 water molecules for a total of 5560 atoms. Thus, our calculation will illustrate that important quantum effects can be included in reaction dynamics studies even for systems of very large size and complexity.

Calculations and Results

The potential energy surface V, which is independent of isotopic substitution, has four terms:

$$V = V_{QM} + V_{QM/MM} + V_{MM} + V_{SEVB} \quad (1)$$

The first three terms are based on a partition into a 54-atom subsystem treated by the quantum mechanical (QM) Austin model 1 (AM1) with parameters from the literature for C, H, N, and O,[23] S,[24] and Zn[25] and a 5506-atom subsystem treated by molecular mechanics with CHARMM-22 parameters for the protein,[26] Zn,[27] coenzyme,[28] and substrate[26] parts of the MM subsystem and T1P3P parameters[29] for the water part of the MM subsystem. The Lorentz−Berthelot combining rules are used to derive parameters for interactions between protein and water atoms. The coupling $V_{QM/MM}$ between the subsystems includes both electrostatic effects and van der Waals terms.[19−21] The QM subsystem includes auxiliary energy terms from four boundary atoms that are treated by a combination of QM and MM using the generalized hybrid orbital method.[21] The AM1 calculations include 160 valence electrons on the benzyl alcoholate anion (which is ligated to the catalytic Zn), the nicotinamide portion of NAD^+ up to the 1′ carbon of ribose, which is a boundary atom, the catalytic Zn, and the ligating portions of three other Zn ligands, in particular the side chains of His-67, Cys-46, and Cys-174 up to their C-α atoms, which are boundary atoms. The MM atoms consist of the structural Zn, 3849 other protein atoms, and the remaining 54 atoms of NAD^+ and 534 water molecules. The semiempirical valence bond (SEVB) term contains a Zn−O valence stretching term and a difference of two extended LEPS equations[30] for the three-body subsystem consisting of transferred H, donor carbon D, and acceptor carbon A. One extended LEPS equation, prefixed by a negative sign, is fit to the AM1 calculations, and the other is fit to ab initio MP2[31] calculations; then a genetic algorithm is used for fine adjustments to make the classical free energy

(10) Miller, W. H. *Adv. Chem. Phys*. **1994**, *25*, 69. To avoid confusion, we mention that throughout the present paper, we use "semiclassical" in the sense of this reference (all degrees of freedom are treated by approximate quantum mechanical methods, and the approximate method used for tunneling is based on approximations motivated by classical limits), as explained in the second paragraph of the present paper. We never use "semiclassical" in the sense that is popular in the kinetic isotope effect community, where it means including zero point effects and vibrational quantization but neglecting tunneling; we call that combination "hybrid". (Thus, the CVT method is hybrid, and CVT/OMT is semiclassical.) In the same spirit of trying to head off confusion, we note that we use "quantum dynamics" to refer to including quantum effects in the nuclear motion; a classical mechanical treatment of nuclear motion based on a quantum mechanical potential function is not called quantum dynamics.

(11) Garrett, B. C.; Truhlar, D. G. *J. Chem. Phys*. **1983**, *79*, 4931.

(12) Kuppermann, A.; Adams, J. T.; Truhlar, D. G. *Abstr. Pap. Int. Conf. Electron. At. Collisions* **1973**, *8*, 149. Marcus, R. A.; Coltrin, M. E. *J. Chem. Phys*. **1977**, *67*, 2609. Skodje, R. T.; Truhlar, D. G.; Garrett, B. C. *J. Phys. Chem*. **1981**, *85*, 3019.

(13) Kreevoy, M. M.; Ostovic, D.; Truhlar, D. G.; Garrett, B. C. *J. Phys. Chem*. **1986**, *90*, 3766. Truhlar, D. G.; Gordon, M. S. *Science* **1990**, *249*, 491.

(14) Liu, Y.-P.; Truong, T. N.; Lu, D.-h.; Truhlar, D. G.; Garrett, B. C. *J. Am. Chem. Soc*. **1993**, *115*, 2408.

(15) Liu, Y.-P.; Lu, D.-h.; González-Lafont, A.; Truhlar, D. G.; Garrett, B. C. *J. Am. Chem. Soc*. **1993**, *115*, 7806.

(16) Allison, T. C.; Truhlar, D. G. In *Modern Methods for Multidimensional Dynamics Computations in Chemistry*; Thompson, D. L., Ed.; World Scientific: Singapore, 1998; p 713.

(17) Garrett, B. C.; Truhlar, D. G. *J. Chem. Phys*. **1979**, *70*, 1593. Truhlar, D. G.; Garrett, B. C. *Acc. Chem. Res*. **1980**, *13*, 440. Truhlar, D. G.; Garrett, B. C. *Annu. Rev. Phys. Chem*. **1984**, *35*, 159. Truhlar, D. G.; Garrett, B. C.; Klippenstein, S. J. *J. Phys. Chem*. **1996**, *100*, 12771.

(18) Warshel, A.; Levitt, M. *J. Mol. Biol*. **1976**, *103*, 227.

(19) Bash, P. A.; Field, M. J.; Karplus, M. *J. Am. Chem. Soc*. **1987**, *109*, 1092.

(20) Gao, J.; Xia, X. *Science* **1992**, *258*, 631.

(21) Gao, J.; Amara, P.; Alhambra, C.; Field, M. J. *J. Phys. Chem. A* **1998**, *102*, 4714.

(22) Alhambra, C.; Gao, J.; Corchado, J. C.; Villà, J.; Truhlar, D. G. *J. Am. Chem. Soc*. **1999**, *121*, 2253.

(23) Dewar, M. J. S.; Zoebisch, E. G.; Healy, E. F.; Stewart, J. J. P. *J. Am. Chem. Soc*. **1985**, *107*, 3902.

(24) Dewar, M. J. S.; Yuan, Y. C. *Inorg. Chem*. **1990**, *29*, 3881.

(25) Dewar, M. J. S.; Merz, K. M. *Organometallics* **1988**, *7*, 522.

(26) Mackerell, A. D.; Bashford, D.; Bellot, M.; Dunbrack, R. L.; Field, M. J.; Fischer, S.; Gao, J.; Guo, H.; Ha, S.; Joseph-McCarthy, D.; Kuchnir, L.; Kuczera, K.; Lau, F. T. K.; Mattos, C.; Michnick, S.; Ngo, T.; Nguyen, D. T.; Prodhom, B.; Reiher, W. E. III; Roux, B.; Schlenkrich, M.; Smith, J. C.; Stote, R.; Straub, J.; Watanabe, M.; Wiorkievicz-Kuczera, J.; Yin, D.; Karplus, M. *J. Phys. Chem. B* **1998**, *102*, 3586.

(27) Stote, R. H.; Karplus, M. *Proteins: Struct., Funct., Genet*. **1995**, *23*, 12.

(28) Paverlites, J. J.; Gao, J.; Bash, P. A.; Mackerell, A. D. Jr. *J. Comput. Chem*. **1997**, *18*, 221.

(29) Jorgensen, W. L.; Chandrasekhar, J.; Madura, J. D.; Impey, R. W.; Klein, M. L. *J. Chem. Phys*. **1983**, *79*, 926.

(30) London, F. *Z. Elektrochem*. **1929**, *35*, 552. Eyring, H.; Polanyi, M. *Z. Phys. Chem*. **1931**, *B12*, 279. Sato, S. *J. Chem. Phys*. **1955**, *23*, 592. Polanyi, J. C. *J. Quant. Spectrosc. Radiat. Transfer* **1963**, *3*, 471. Kuntz, P. J.; Nemeth, E. M.; Polanyi, J. C.; Rosner, S. D.; Young, C. E. *J. Chem. Phys*. **1966**, *44*, 1168.

(31) Krishnan, R.; Pople, J. A. *Int. J. Quantum Chem*. **1978**, *14*, 91.

of activation approximately match experimental[32] data. Further details of the parametrization of the SEVB term are given in the Computational Section. The SEVB potential adjusts the shape of the one-dimensional potential of mean force (PMF) along the reaction coordinate, especially for the overall exoergicity and barrier height, but—since it depends only on four internuclear distances—it cannot be used for general adjustments of the coupling of vibrational modes to the reaction coordinate. Thus, the calculations reported in this paper, which are sensitive to this coupling, will test the adequacy of the AM1-GHO-CHARMM22-TIP3P potential (combined with variational transition-state theory with multidimensional tunneling calculations) for predicting these detailed aspects of the dynamics.

The dynamics are treated by stochastic boundary conditions.[33] A reaction zone of radius 20 Å (centered on the midpoint of a line from the donor carbon *D* to the acceptor carbon *A*) is treated without constraints. A shell from 20 to 24 Å forms a buffer zone and is treated by constrained Langevin dynamics.[33,34] Residues and solvent molecules beyond 24 Å are omitted. LADH is a dimer containing 748 residues and 4 Zn atoms. This treatment includes 239 residues and 2 Zn atoms from one monomer unit and 21 residues and no Zn from the other plus, as stated above, 534 water molecules.

We carried out calculations for the present system for six isotopic combinations, just as in the experiments.[1,2] Our notation is that $k_{\mathrm{Pr}}^{\mathrm{Se}}$ is the rate constant for

$$\mathrm{LADH{\cdot}PhCPrSeO^{-}\cdots NAD^{+} \rightarrow LADH{\cdot}PhCSeO\cdots NADPr}$$

where Pr and Se are the primary and secondary hydrogen atoms or their isotopes; Pr denotes H(1°), D(1°), or T(1°), and Se denotes H(2°), D(2°), or T(2°).

The dynamics calculations involve two stages. In the first stage, the reaction zone is classical, and there are two substages. In the first substage, we calculate the PMF (also called the free energy profile) $W(z)$ as a function of the distinguished coordinate z defined by

$$z = r_{HD} - r_{HA} \tag{2}$$

where r_{HX} is the distance between the transferred H and atom X. The calculation employs umbrella sampling[35] and yields $W(z)$ in windows spaced by 0.25 Å. Figure 1 shows the average of V_{QM} over configurations sampled along the reaction path and compares it with the PMF for the hydride-transfer reaction. This energy change is −14 kcal/mol, but the computed PMF, which includes enzyme−substrate interactions and dynamic fluctuations, shows a nearly ergoneutral reaction. The PMF shows a free energy of activation of 16 kcal/mol for the hydride-transfer step of the enzymatic reaction. The corresponding experimental activation barrier is 15.6 kcal/mol.[32]

The highest-W window is selected for further sampling in the second substage. First we compute $\langle r_{HD} \rangle$ and $\langle r_{HA} \rangle$ for this window. Then we carry out a constrained sample with these two distances harmonically constrained close to their average, and after 20 ps of equilibration, we randomly select 20 configurations at random, ~2.5 ps apart, for further use in stage 2.

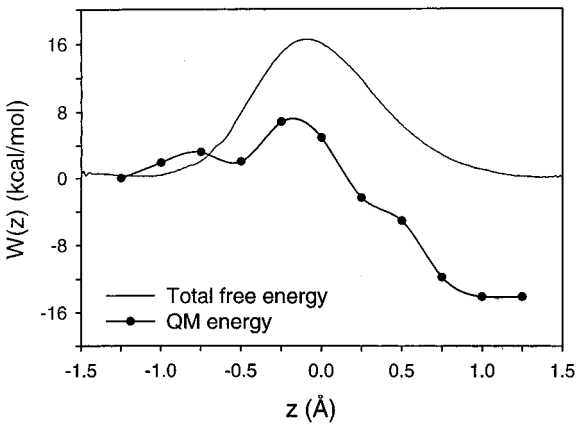

Figure 1. Free energy profile of entire system compared to internal energy of the 54-atom subsystem, as functions of the reaction coordinate.

Although the present work takes the hydrogen atom position as the distinguished coordinate for stage 1, alternative treatments could be based on a collective solvent coordinate[36−39] such as the one used in the Marcus theory of electron transfer. This issue is discussed at length in another paper.[40] Looking ahead, we note that the distinguished coordinate is only used in stage 1; the stage 2 reaction coordinate will not involve preselection of a distinguished coordinate.

In stage 2, the system is divided into a primary zone and a secondary zone. The primary zone has 21 atoms and consists of $C-CH_2O^-$ from the alcoholate, the Zn, and the entire nicotinamide portion of NAD^+; the secondary zone consists of the rest. For each of the configurations selected in stage 1, we freeze the secondary zone,[41] calculate the minimum energy path (MEP) of primary zone atoms in mass-weighted coordinates, and calculate the rate constant by CVT/OMT using the embedded cluster[42] algorithm. In this way, 63 degrees of freedom are treated by semiclassical quantum dynamics in the field of a 5539-atom secondary zone. The small-curvature approximation is selected for the OMT calculations on the basis of variational calculations for energies from 0 to 2.1 kcal/mol below the barrier top (large-curvature tunneling calculations are very sensitive to some of the approximations for even lower energies, but these contribute negligibly in the present calculations). The fact that the small-curvature approximations are variationally preferred to the large-curvature one for this system may seem surprising since the transfer of a light particle between two heavy moieties is often associated with large reaction-path curvature; however, as discussed elsewhere,[43] that correlation is strictly valid only for bimolecular reactions (where the

(32) Sekhar, V. C.; Plapp, B. V. *Biochemistry* **1990**, *29*, 4289. Shearer, G. L.; Kim, K.; Lee, K. M.; Wang, C. K.; Plapp, B. V. *Biochemistry* **1993**, *32*, 11186.

(33) Brooks, C. L.; Brunger, A.; Karplus, M. *Biopolymers* **1985**, *24*, 843. Brooks, C. L.; Pettitt, B. M.; Karplus, M. *J. Chem. Phys*. **1985**, *83*, 5897.

(34) Chandresekhar, S. *Rev. Mod. Phys*. **1943**, *15*, 1.

(35) Valleau, J. P.; Torrie, G. M. In *Statistical Mechanics, Part A*; Berne, B. J., Ed.; Plenum: New York, 1977; p 137.

(36) Marcus, R. A. *Discuss. Faraday Soc*. **1960**, *29*, 21.

(37) Lee, S.; Hynes, J. T. *J. Chem. Phys*. **1988**, *88*, 8863.

(38) Yadav, A.; Jackson, R. M.; Holbrook, J. J.; Warshel, A. *J. Am. Chem. Soc*. **1991**, *113*, 4800.

(39) Truhlar, D. G.; Schenter, G. K.; Garrett, B. C. *J. Chem. Phys*. **1993**, *98*, 5756.

(40) Schenter, G. K.; Garrett, B. C.; Truhlar, D. G., to be published.

(41) The validity of freezing the secondary zone on the time scale of the reactive event has been examined recently by Neria and Karplus (Neria, E.; Karplus, M. *Chem. Phys. Lett*. **1997**, *267*, 23. Karplus, M. *J. Phys. Chem. B* **2000**, *104*, 11) in classical mechanical simulations of proton transfer catalyzed by triose phosphate isomerase. They compared calculations with frozen and unfrozen baths with an even smaller primary zone than used here and found that the dynamics of environmental atoms is unimportant for calculating the transmission coefficient. One expects larger effects on the free energy of activation and reorganization energy, and the magnitude of these quantities also affects the quantum effects.

(42) Lauderdale, J. G.; Truhlar, D. G. *J. Chem. Phys*. **1986**, *84*, 1843. Wonchoba, S. E.; Truhlar, D. G. *J. Chem. Phys*. **1993**, *99*, 9637.

(43) Truhlar, D. G. *J. Chem. Soc., Faraday Trans*. **1994**, *90*, 1740.

Table 1. Primary and Secondary Kinetic Isotope Effects and Exponents

		TST[a]	CVT[a]	CVT/OMT[a]	expt[b]
primary	k_H^H/k_T^H	6.1 ± 0.4	5.9 ± 0.5	6.2 ± 0.9	7.1 (7.3−7.8)
	k_D^D/k_T^D	1.73 ± 0.03	1.72 ± 0.03	1.8 ± 0.1	1.9 (1.8−1.9)
secondary	k_H^H/k_H^T	1.09 ± 0.01	1.10 ± 0.02	1.29 ± 0.04	1.33 (1.31−1.32)
	k_D^D/k_D^T	1.03 ± 0.00[c]	1.03 ± 0.01	1.06 ± 0.01	1.07 (1.03−1.05)
exponent[d]	α_{prim}	3.30 ± 0.01	3.25 ± 0.06	3.2 ± 0.2	3.1 (3.3)
	α_{sec}	3.3 ± 0.2	3.4 ± 0.4	4.4 ± 0.3	4.1 (6.1−8.5)

[a] All calculations for wild-type at 300 K. [b] Reference 2; wild-type value is shown first followed by values for mutants in parentheses. [c] 1.027 ± 0.003. [d] Computed from unrounded kinetic isotope effects.

entrance valley is aligned with a vector from the center of mass of one reagent to the center of mass of the other) whereas the present system is unimolecular.

The Swain−Schaad exponents[44] are

$$\alpha_{prim} = \frac{\ln(k_H^H/k_T^H)}{\ln(k_D^D/k_T^D)} \quad (3)$$

$$\alpha_{sec} = \frac{\ln(k_H^H/k_H^T)}{\ln(k_D^D/k_D^T)} \quad (4)$$

The importance of the exponents is that they were used by Klinman and co-workers[1−3] as an indicator for tunneling. In particular, $\alpha > 3.3$ (this upper limit of "normal" behavior is based on the assumptions[44] of transition-state theory, uncoupled harmonic stretch motions, the same transition-state geometry for all isotopes, and no tunneling) was considered to be an indication of an enhanced reaction rate due to tunneling increasing the rate constant significantly for the lightest mass combination but much less so for the others.

We carried out calculations for 20 secondary-zone configurations for each of the 6 isotopic combinations appearing in eqs 1 and 2. The kinetic isotope effects (KIEs) and Swain−Schaad exponents were averaged over all 20 secondary-zone configurations, and the resulting averages and standard deviations are given in Table 1. For comparison with the final CVT/OMT results, rate constants were also calculated by conventional transition-state theory (TST)[45] and by CVT with quantized vibrations but without tunneling. Calculations with a 31-atom primary zone in which we unfroze the entire benzyl group (resulting in 93 degrees of freedom treated by semiclassical quantum dynamics) agree with the values in Table 1 within a few percent.

The most serious approximation in the present work may be the neglect of the secondary-zone entropy. By averaging over secondary-zone structures, we have included the internal energy effect of secondary-zone fluctuations but not the entropic part. In a subsequent paper, we will present a third-stage algorithm for including this effect. The method employed by Hwang and Warshel (1996, ref 9) includes a more complete treatment of protein fluctuations but a less complete treatment of quantum effects.

Table 1 also compares the kinetic isotope effects and exponents to experiment.[2] The experimental numbers are affected by kinetic complexity due to the fact that, at least for the wild-type case, the rate is partially limited byproduct benzaldehyde dissociation. Some idea of the intrinsic values for the catalytic step is provided by the values for mutants; these values are given in parentheses; for the mutants, the catalytic step is fully or more fully rate-determining. The operational assumption is that the true result for the rate-determining step in wild-type LADH (which is simulated here) is somewhere in or near the range of the wild-type and mutant values. The X-ray structure for one of the mutants (F93W) is virtually superimposable on the wild-type structure.

Discussion

The agreement between theory and experiment in Table 1 is better than one has a right to expect because the experimental numbers are affected by kinetic complexity and because of the size of the system and the many interactions contributing to free energy changes along the reaction path. Nevertheless, the good agreement is very gratifying and encouraging, and it gives us confidence in the detailed picture of the tunneling process provided by the calculations, as discussed next.

For the more detailed analysis that follows, we selected the most typical secondary-zone configuration (that agrees best with all the average kinetic isotope effects and Swain−Schaad exponents), and we will base further discussion on this typical case (because the component numbers fit together in a less confusing fashion when one discusses a typical configuration than when one works with the averages—but all qualitative conclusions are unaffected).

We denote the transmission coefficient as κ_{Pr}^{Se} for a given primary (Pr) and secondary (Se) isotopic hydrogen. The calculations indicate that $\kappa_H^H = 2.34$, $\kappa_T^H = 2.35$, and $\kappa_H^T = 2.02$. It is not a round-off error that the "expected" trend, $\kappa_H^H > \kappa_T^H$, is *not* observed for primary substitution. Similarly, the expected trend $\kappa_H^T > \kappa_D^T$ is not observed because $\kappa_D^T = 2.18$. Those trends are only guaranteed if the effective potential and tunneling path are isotope independent, but they are not isotope independent for multidimensional tunneling. (Multidimensional tunneling approximations account for the coupling of other modes to the nominal reaction coordinate both in terms of determining the optimum tunneling paths and in terms of determining the effective potentials and reduced masses along those paths; an introductory explication is available elsewhere.[46]) Indeed there are now several theoretical calculations in the literature where $\kappa_D > \kappa_H$ for primary substitution in nonenzymatic[47] and enzymatic[22] reactions. For the present perprotio reaction, the dominant tunneling energy is 0.40 kcal/mol below the effective barrier top. At this energy, the tunneling path starts with $r_{HD} = 1.14$ Å, $r_{HA} = 1.49$ Å; and it terminates at $r_{HD} = 1.31$ Å, $r_{HA} = 1.28$ Å. Figure 2 shows five structures at critical points along

(44) Swain, C. G.; Stivers, E. C.; Reuwer, J. F.; Schaad, L. J. *J. Am. Chem. Soc.* **1958**, *80*, 5885. Saunders, W. H., Jr. *J. Am. Chem. Soc.* **1985**, *107*, 164. Huskey, W. P. *J. Phys. Org. Chem.* **1991**, *4*, 361.

(45) Eyring, H. *J. Chem. Phys.* **1935**, *3*, 107.

(46) Tucker, S. C.; Truhlar, D. G. In *New Theoretical Concepts for Understanding Organic Reactions*; Bertrán, J., Csizmadia, I. G., Eds.; NATO ASI Series C 267; Kluwer: Dordecht, 1989; pp 291−346.

(47) Truong, T. N.; McCammon, J. A. *J. Am. Chem. Soc.* **1991**, *113*, 7504. Storer J. W.; Houk, K. N. *J. Am. Chem. Soc.* **1993**, *115*, 10426. Corchado J. C.; Espinosa-Garcia, J. *J. Chem. Phys.* **1996**, *105*, 3160. Villá, J.; González-Lafont, A.; Lluch, J. M. *J. Phys. Chem.* **1996**, *100*, 19389. Hu, W.-P.; Rossi, I.; Corchado, J. C.; Truhlar, D. G. *J. Phys. Chem. A* **1997**, *101*, 6911.

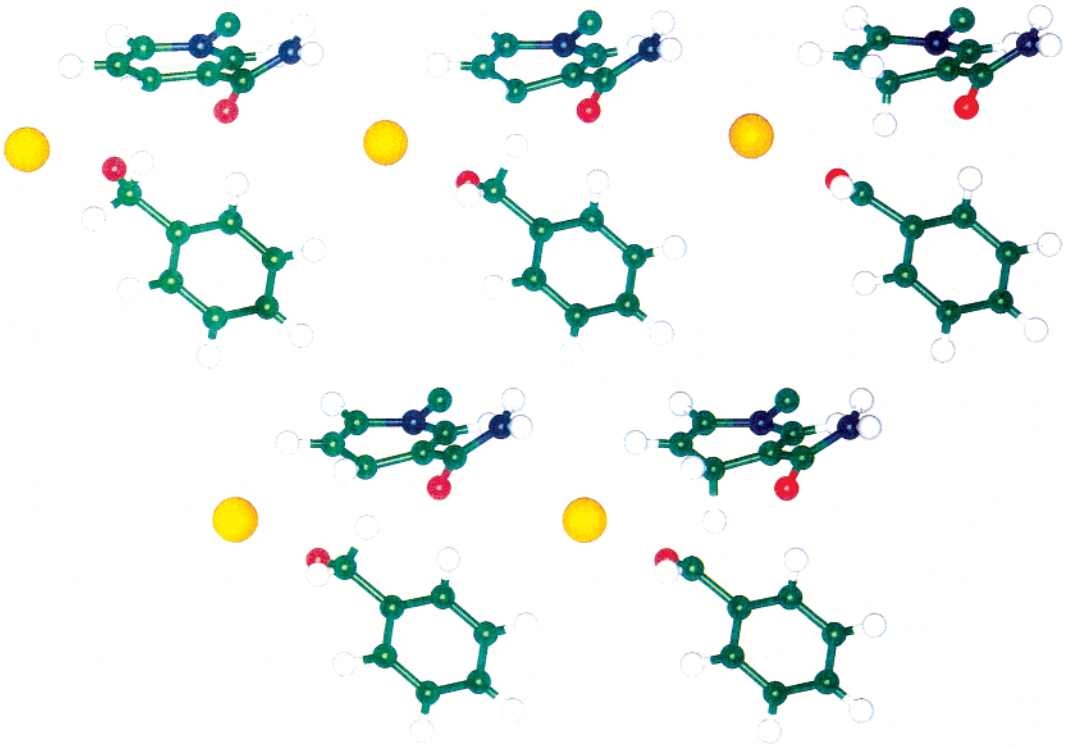

Figure 2. Five snapshots of the primary zone and the attached C of ribose. The top row shows reactant, transition state, and product. The bottom row shows the starting and ending termini of the dominant tunneling path. Thus, the time sequence of the "movie" is upper left (reactant), lower left ($s = -0.19$ amu$^{1/2}$ Å), center ($s = -0.03$ amu$^{1/2}$ Å), lower right ($s = 0.07$ amu$^{1/2}$ Å), upper right (product).

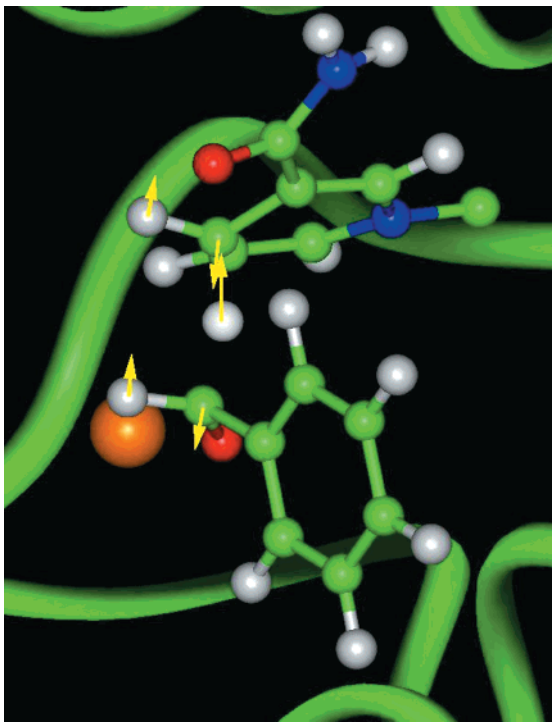

Figure 3. Reaction-coordinate normal mode at the transition state.

the reaction path, and this provides a moving picture of the tunneling process and shows that heavy atom motions are smaller than the hydride motion, especially during the tunneling event. Rehybridizations of the benzylic and NAD C-4 carbon atoms accompanying the hydride transfer are clearly seen in Figure 2. These coupled dynamic motions that make up the reaction coordinate are depicted in Figure 3, which is a graphical representation of the imaginary-frequency normal mode. This mode shows predominant motion of the donor and acceptor atoms, the transferred H along the axis connecting them, and the coupled bending motions of secondary hydrogen atoms. The calculated reactive flux suggests that at least 57% of the reaction goes by tunneling.

Table 1 shows that the magnitudes of the primary KIEs are well accounted for by conventional transition-state theory. It is interesting to compare the full calculations to the simplest model, according to which the KIE is due to the decrease along the reaction path of a single frequency associated with the broken bond. For k_H^H, the frequency of the mode that evolves from the breaking C−H bond stretch to the quasisymmetric combination of the breaking and forming C−H bond stretches decreases from 2895 cm^{-1} at reactants to 1913 cm^{-1} at the saddle point, whereas the corresponding frequencies for k_T^H are 1762 and 1721 cm^{-1}, respectively. The zero point energy of this mode would thus account for a KIE of 9.7, which must be partially compensated by other changes, since the full TST model yields 6.0. The one-mode, conventional-TST model for the secondary KIE yields 1.08 (based on frequencies of 1873 and 1138 cm^{-1} for k_H^H and 1168 and 1138 cm^{-1} for k_H^T), which is qualitatively correct.

The quantum mechanical tunneling effect is clearly revealed by the computed secondary KIE in Table 1. Without tunneling, the predicted secondary k_H^H/k_T^H KIE at the CVT level of theory is 1.10, which is much smaller than the experimental value. Good agreement with experiment is obtained only when tunneling corrections are included in the theory. Table 1 also shows that the exhalted Swain−Schaad exponent for the secondary kinetic isotope effect results entirely from tunneling, which (as is easily calculated from κ_H^H and κ_T^H given above) increases the H/T secondary KIE by 16%.

One advantage of the semiclassical method used here is that we can dissect the origin of the exhaltation of the exponent in more detail. The imaginary frequencies at the saddle point for k_H^H and k_H^T are 1046i and 1002i cm^{-1}. These values are

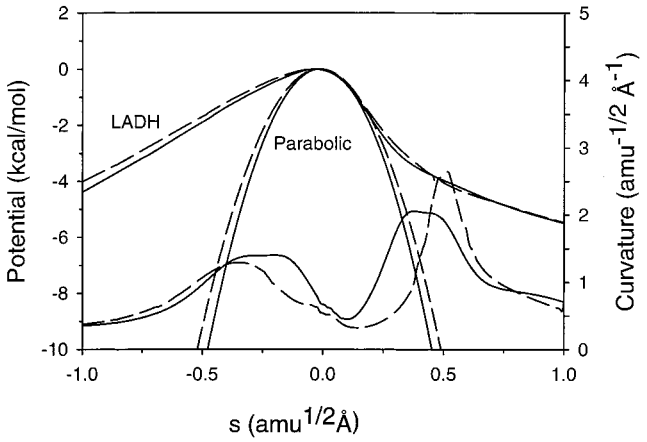

Figure 4. Effective potential for tunneling (scale at left), parabolic approximation to the effective potential based on the saddle point imaginary frequency (scale at left), and curvature of the MEP (scale at right), all as functions of distance *s* along the MEP. The effective potentials and parabolic approximations are all normalized to zero at their highest point to facilitate comparison. Results are shown for the k_H^H (solid curves) and k_H^T processes (dashed curves).

insufficient to calculate κ quantitatively because they quantify the width of the barrier only near its top, whereas κ_H^H is dominated by tunneling at energies 0.4 kcal/mol below the top, where the barrier is much wider than its parabolic approximation. In particular, the vibrationally adiabatic ground-state potential energy barrier (which includes[46,48−51] the changes in zero point energies of modes transverse to the reaction coordinate) for k_H^H is 0.26 amu$^{1/2}$ Å wide and that for k_H^T is 0.28 amu$^{1/2}$ Å wide as compared to 0.19 and 0.20 for the parabolic approximations. The barrier is primarily widened on the reactant side of the barrier, as shown in Figure 4. In this region, the reaction path calculations employing the true vibrationally adiabatic potential for each isotopic case but assuming that the tunneling path is along the MEP[48] (which would be true for zero curvature of the MEP) yield $\kappa_H^H = 1.61$ and $\kappa_H^T = 1.50$, an 8% effect. The other 8% comes from reaction path curvature, which is larger for k_H^H than for k_H^T in the region of the dominant tunneling paths, as is also shown in Figure 4. For example, the reaction path curvature at the critical location 0.16 amu$^{1/2}$ Å before the barrier is 1.7 times larger for k_H^H than for k_H^T. Thus, the same tunneling models that have been successfully validated for small-molecule reactions[14−16] predict a secondary kinetic isotope effect in good agreement with experiment for LADH with no new assumptions. To compare precisely with experiment requires considering κ_D^D and κ_D^T as well, for which we calculate 2.23 and 2.18, respectively. The fact that $\kappa_D^T > \kappa_H^T$ has a large quantitative effect on the Swain−Schaad exponent, but it is intrinsically a multidimensional effect. We conclude that the multidimensional aspect of tunneling is paramount for quantitative modeling of these KIEs.

The most thorough previous attempt to explain the detailed kinetic isotope effects in this system is provided by the work of Rucker and Klinman.[52] They assumed that the transition-state force constants can be interpolated from reactant and product force constants and obtained best-fit constants by using transition-state theory with a parabolic one-dimensional tunneling model. To satisfactorily reproduce the k_H^H/k_H^T secondary kinetic isotope effects, they required a model in which the effect computed without tunneling is very small (1.01). As a result, this kinetic isotope effect was interpreted as arising almost entirely from one-dimensional tunneling along a coupled-motion reaction coordinate, and this resulted in the secondary kinetic isotope effects exhibiting a normal (nonexalted) Swain−Schaad exponent. The present treatment, by including nonparabolic multidimensional tunneling, indicates that the root problem in the treatment of ref 52 is the overestimation of the tunneling by the parabolic one-dimensional tunneling approximation. The present treatment predicts less tunneling, shows that the k_H^H/k_H^T secondary kinetic isotope effect is nonnegligible (1.10) even in the absence of tunneling, and yields an exalted Swain−Schaad exponent in qualitative agreement with experiment. In other words, the present treatment, for the first time, is able to reproduce both k_H^H/k_H^T and k_H^D/k_H^T. These kinetic Isotope effects are not reproduced when we neglect tunneling, and thus our calculations confirm the essential correctness of the contention of Klinman and co-workers[1−3] that the elevated Swain−Schaad exponent for secondary kinetic isotope effects in the hydride-transfer step of alcohol dehydrogenases is experimental evidence for the importance of hydrogen tunneling in enzyme catalysis.

Whence the exaltation? The present study leads to a simple picture of the critical portion of the tunneling process that is responsible for exhaltation of the secondary H/T Swain−Schaad exponent. At the start of the reactive event, the *A* and *D* atoms move closer. Then the *D*−H bond begins to break. At this point there is significantly more tunneling when the secondary H is not replaced by T, about half of which is due to a narrower barrier attributable to secondary hydrogen participation in the minimum energy path and about half of which is due to greater opportunities for corner-cutting tunneling because the reaction path is more curved in isoinertial coordinates.

Computational Section

The only parameters specifically optimized for this study are those in V_{SEVB}. In the present work, the SEVB term is itself a sum of three terms

$$V_{SEVB} = \frac{1}{2}k(r_{O-Zn} - r_o)^2 - V_L^{(1)} + V_L^{(2)} \qquad (5)$$

where k and r_o are parameters and $V_L^{(i)}$ is an extended London−Eyring−Polanyi−Sato (LEPS) three-body potential energy function[30] involving the transferred H^- atom (H), the donor carbon (D) of the alcohol, which is the methylene carbon, and the acceptor carbon (A) of NAD^+, which is C(4). The two extended LEPS functions have different parameters, and they each depend on the three interatomic distances r_{HD}, r_{HA}, and r_{AD}. The difference of LEPS terms for a three-body subsystem is in the spirit of an IMOMO improvement of the subsystem.[53]

Without V_{SEVB}, the GHO-AM1/CHARMM-22 potential function exhibits two qualitative deficiencies: (1) In the product ternary complex, the bond between the catalytic Zn and the aldehyde oxygen is too weak to be stable, whereas an X-ray structure[54] of an LADH/NADH/*N*-cyclohexylformamide ternary complex (which is presumed to mimic the ternary aldehyde complex) shows a 2.3-Å Zn−O distance, and strong interaction of the carbonyl group of Zn is confirmed[55] by a Raman experiment. (Ab initio Hartree−Fock theory also overestimates

(48) Truhlar, D. G.; Kuppermann, A. *J. Am. Chem. Soc*. **1971**, *93*, 1840.
(49) Garrett, B. C.; Truhlar, D. G.; Grev, R. S.; Magnuson, A. W. *J. Phys. Chem*. **1980**, *84*, 1730.
(50) Truhlar, D. G.; Isaacson, A. D.; Skodje, R. T.; Garrett, B. C. *J. Phys. Chem*. **1982**, *86*, 2252.
(51) Kreevoy, M. M.; Truhlar, D. G. In *Investigation of Rates and Mechanisms of Reactions*, 4th ed.; Bernasconi, C., Ed.; Techniques of Chemistry Series Vol. 6; Wiley: New York, 1986; Part I, pp 13−95.
(52) Rucker, J.; Klinman, J. P. *J. Am. Chem. Soc.* **1999**, *121*, 1997.
(53) Humbel, S.; Sieber, S.; Morokuma, K. *J. Chem. Phys.* **1996**, *16*, 1959. Coitiño, E. L.; Truhlar, D. G.; Morokuma, K. *Chem. Phys. Lett.* **1996**, *259*, 159.
(54) Ramaswamy, S.; Scholze, M.; Plapp, B. V. *Biochemistry* **1997**, *36*, 3522.

Zn−O distances for aldehyde coordination.) (2) The overall free energy change of the reaction is calculated to be −20 kcal/mol, rather than +1.

The first term in V_{SEVB} was added to correct the first deficiency. We set $k = 40$ kcal mol^{-1} Å^{-2} and $r_o = 2.29$ Å, which reduces the Zn−O distance to 2.38−2.39 Å for typical configurations.

The next two terms of V_{SEVB} correct the overall exoergicity of the potential energy function because the QM/MM method that we are using is not accurate enough to yield the correct energy of reaction. Both of these terms have the form of extended London−Eyring−Polanyi−Sato three-body potentials,[30] which are functions of the interatomic distances r_{HD}, r_{HA}, and r_{AD} that are involved in bond breaking and bond making. In particular

$$V_L = Q_{HD} + Q_{HA} + Q_{AD} - \{0.5[(J_{HD} - J_{HA})^2 + (J_{HA} - J_{AD})^2 + (J_{AD} - J_{HD})^2]\}^{1/2} \quad (6)$$

where the Coulomb integral between atoms X and Y is

$$Q_{XY} = 0.5[V_-(r_{XY}) + V_+(r_{XY})] \quad (7)$$

and the exchange integral between atoms X and Y is

$$J_{XY} = 0.5[V_+(r_{XY}) - V_-(r_{XY})] \quad (8)$$

The functions V_- and V_+ are Morse and anti-Morse curves given respectively by

$$V_-(r_{XY}) = D_{XY}\{\exp[-2\beta_{XY}(r_{XY} - r_{e,XY})] - 2\exp[-\beta_{XY}(r_{XY} - r_{e,XY})]\} \quad (9)$$

and

$$V_+(r_{XY}) = 0.5\frac{1 - Z_{XY}}{1 + Z_{XY}}D_{XY}\{\exp[-2\beta_{XY}(r_{XY} - r_{e,XY})] + 2\exp[-\beta_{XY}(r_{XY} - r_{e,XY})]\} \quad (10)$$

where D_{XY}, β_{XY}, and $r_{e,XY}$ are Morse parameters and Z_{XY} is a Sato parameter. Thus, there are four parameters per diatomic pair in $V_L^{(1)}$ and the same number in $V_L^{(2)}$ for a total of 24 parameters.

In the general case, all 24 parameters could be adjusted in any fashion that is useful to improve the potential energy surface; in the present paper though, we constrained most of them by calculations on model systems. First, we carried out AM1, ab initio, and density functional calculations on the following model reaction:

$$NMN^+ + PhCH_2O^- \rightarrow NMNH + PhCHO \quad (R1)$$

where NMN^+ denotes N_1- methyl nicotinamide cation, and Ph denotes phenyl. Table 2 gives the zero-point-exclusive energy of reaction ΔE at the AM1,[23] MP2,[31] and B3LYP[56] levels of electronic structure theory, where the latter two calculations employ the 6-31+G* [57] basis set. This table clearly shows that the AM1 method overestimates the exoergicity in the gas phase by an amount comparable to the error in the enzyme simulation. We concluded that this is the main reason the GHO-AM1/CHARMM22 calculations gave $\Delta G = -20$ kcal/mol, whereas the experimental result is $\Delta G = +1$ kcal/mol, Thus, the semiempirical valence bond correction term is used primarily to make up for the deficiency of AM1.

Table 2. Energetics of Reaction R1

level	ΔE (kcal/mol)
AM1	−146.9
MP2/6-31+G*	−128.0
B3LYP/6-31G*//MP2/6-31+G*	−128.6

Table 3. Morse Parameters Fit to Calculations on Model Reaction

	(1) AM1		(2) MP2	
	HA	HD	HA	HD
D_{XY} (kcal/mol)	245.25[a]	98.3[a]	220.20[a]	92.20[a]
$r_{e,XY}$ (Å)	1.127	1.148	1.0857	1.1160
β_{XY} (Å^{-1})	1.301[b]	1.9226	1.4771	1.9811

[a] This value is increased by 10% for the final surface. [b] This value is changed to 1.501 for the final surface.

Table 4. Parameters Adjusted To Give a Realistic Energy Profile along the Reaction Path

	(1)			(2)		
	HA	HD	AD	HA	HD	AD
D_{XY}	269.77	108.30	26.30	238.22	101.42	7.402
β_{XY}	1.501	1.923	0.675	1.4471	1.9811	0.3390
Z_{XY}	0.02231	−0.01449	0.0	−0.02451	0.02063	0.0

As a starting point for correcting the potential energy surface, we assume that the correction in the enzyme is the same as the difference between the AM1 and MP2 calculations for model reaction R1. Thus, the initial set of parameters for $V_L^{(1)}$ is taken from the AM1 calculations on the model reaction, and the initial parameters for $V_L^{(2)}$ are taken from the MP2 calculations on the model reaction. In particular, $V_\pm(r_{HA})$ represents $NMNH \rightarrow NMH^+ + H^-$ and $V_\pm(r_{HD})$ represents $PhCH_2O^- \rightarrow PhCHO + H^-$. These parameters are given in Table 3. The values of D_{AD}, $r_{e,AD}$, and β_{AD} as well as all the Sato parameters were taken as adjustable parameters and are adjusted by a genetic algorithm[58] to give the minimum value for an unfitness function designed to give reasonable values for the barrier height and endoergicity. We also increased β_{HA} by 0.2 Å to fine-tune the energy contours in the reactant valley of the potential energy surface, and we increased all the D_{HA} and D_{HD} values by 10% to give a better energy profile along the reaction path. The final values of the parameters adjusted in this process are given in Table 4.

Acknowledgment. This work was supported in part by the National Science Foundation and by the National Institutes of Health, the Center for Computational Research of the State University of New York at Buffalo, and the University of Minnesota Supercomputer Institute.

JA001476L

(55) Deng, H.; Schindler, J. F.; Berst, K. B.; Plapp, B. V.; Callender, R. *Biochemistry* **1998**, *37*, 14267. Callender, R.; Chen, D.; Lugtenburg, J.; Martin, C.; Rhee, K. W.; Sloan, D.; Vandersteen, R.; Yue, K. T. *Biochemistry* **1988**, *27*, 3672.

(56) Stephens, P. J.; Devlin, F. J.; Ashvar, C. S.; Bak, K. L.; Taylor, P. R.; Frisch, M. J. *ACS Symp. Ser.* **1996**, *No. 629*, 105.

(57) Hehre, W. J.; Radom, L.; Schleyer, P. v. R.; Pople, J. A. *Ab Initio Molecular Orbital Theory*; Wiley: New York, 1986.

(58) Carroll, D. L. *AIAA J.* **1996**, *34*, 338. We used version 1.6.4 of Carroll's code from http://www.staff.uiuc.edu/carroll./ga.html (January, 1997).